PCCP

ROYAL SOCIETY OF CHEMISTRY

PAPER

View Article Online
View Journal | View Issue

Cite this: *Phys. Chem. Chem. Phys.*, 2025, **27**, 5821

Unique catalytic role of intermolecular electric fields that emanate from Lewis acids in a ring closing carbonyl olefin metathesis reaction†

Lopita Swain, Karthik Gopakumar and Rajeev Ramanan *

Electric field (EF) catalysis has evolved as an effective tool for controlling reactivity and selectivity of reactions. While EF catalysis brings precise control over reactivity, it also challenges the concept's practical realization due to the difficulties in juxtaposing reactants with directional EF. The present density functional theory (DFT) studies demonstrate the catalytic role of the inherent intermolecular EFs that originate from Lewis acids (LA) during a ring-closing carbonyl–olefin metathesis (RCCOM) reaction. The specificity of LA coordination to reactants generates specifically oriented intermolecular EF components along the reaction axis which is defined parallel to the direction of flow of electrons wherein the influence of the EF would be at maximum. By examining the thermal [2+2] cycloaddition and carbonyl–ene reaction steps in a RCCOM reaction as model systems, the results revealed the pivotal role of intermolecular EF in mixing some of the dormant ionic structures into normal covalent structures and facilitating a partial rotation of the nonbonding orbitals at the carbonyl oxygen to enhance an ionic pseudo-pericyclic pathway. The unique role of intermolecular EF is further verified by modelling the pristine reaction, in the absence of LAs, under oriented external EFs. The conspicuous intermolecular EF component adds to other modes of catalysis, such as conventional Lewis acidity, to result in the gross catalytic effect. The findings offer insights into the practical realization of EF catalysis by harnessing the intermolecular EFs and point out the need to include intermolecular EF as an inevitable factor for a holistic explanation of any catalytic mechanism.

Received 28th December 2024,
Accepted 14th February 2025

DOI: 10.1039/d4cp04879b

rsc.li/pccp

1. Introduction

Oriented external electric fields (EFs) are future smart reagents and invisible catalysts for chemical reactions.[1] The mechanism of oriented external EFs acting as an invisible catalyst in chemical reactions has been explained by theory and demonstrated by experiments.[2–12] Oriented external EF as a stimulus imparts changes in structure, bonding, electronic states, and the reaction outcome.[2] The details on the impact of an oriented external EF on chemical reactions such as the Diels–Alder reaction,[7,8] C–H bond activation,[9] methyl transfer,[10] disproportionation of methanol into methane and formaldehyde,[11] nucleophilic substitution,[12] electrophilic aromatic substitution,[13] modulating entropy,[14] and pH effects[15] in water, oxidative addition,[16] and catalyst free hydrogen synthesis[17] were reported. EF can selectively polarize molecules, modify solvation dynamics, and stabilize reactive intermediates, improving catalytic efficiency. EF-induced electro-freezing can also restrict the dynamics of the hydrogen bond network in water and result in a ferroelectric amorphous phase.[18] Recent advancements in utilizing the inherent internal EFs in water microdroplet chemistry have generated a novel approach to harness EF catalysis in chemical reactions.[19–24] The naturally occurring high EFs at the peripheries of water microdroplets serve as a highly efficient catalyst for a range of reactions such as proton transfer,[25] halogen-bond breaking,[20] nucleophilic addition,[21] alkylation,[22] photolysis of H_2O_2,[23] methane oxidation[24] and cross-coupling reactions between C–H and N–H bonds.[26] However, some reports suggest that Diels–Alder reactions in water microdroplets which are driven by rapid evaporation and reagent enrichment have minor EF contribution towards the gross catalysis.[27] Nature utilizes a preorganised intrinsic EF within enzymes to bring efficient catalysis.[6] Tailoring charged functional groups on the porphyrin ring was effective in catalysing hydrogen atom transfer reactivity of the ferryl [Fe(IV)-oxo] in metalloenzyme analogues due to the generation of an oriented intrinsic EF.[28,29] As such, catalysis that utilizes the intrinsic EF is a promising area and it opens up a new avenue for the practical use of EF catalysis.

Department of Chemistry, National Institute of Technology Rourkela, Odisha, 769008, India. E-mail: rrajeev@nitrkl.ac.in

† Electronic supplementary information (ESI) available: The intermolecular EF values, group charges, molecular orbital energies, energies and cartesian coordinates of the optimized geometries. See DOI: https://doi.org/10.1039/d4cp04879b

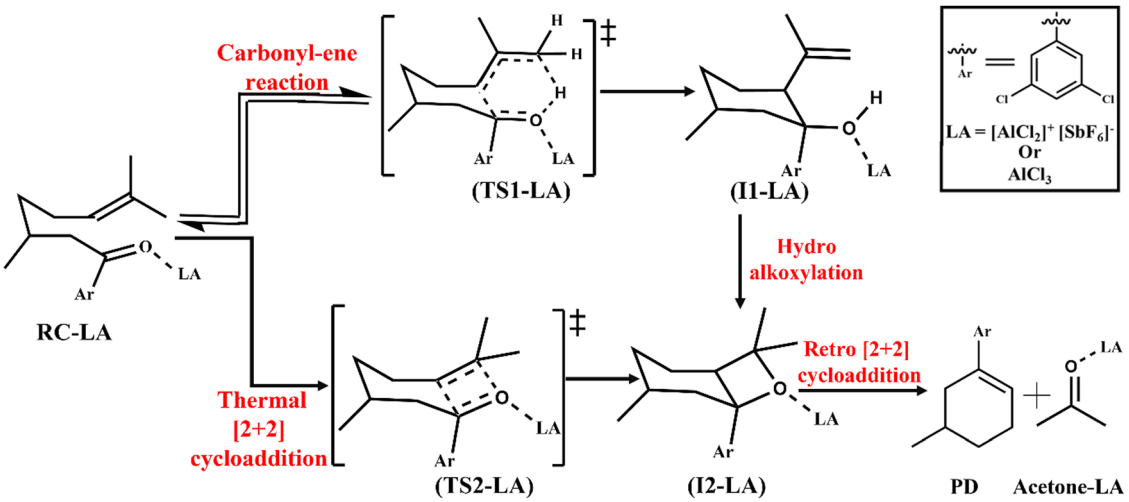

Scheme 1 Mechanistic details of the RCCOM reaction catalysed by the LA.

The present study provides a comprehensive analysis of the role of intermolecular EF emanating from a Lewis acid (LA) in a [2+2] cycloaddition as well as in the competitive carbonyl–ene reaction that occurs concurrently in a ring-closing carbonyl–olefin metathesis (RCCOM) reaction. In the following discussion, we quantified the intermolecular EF generated by two LA catalysts, $[AlCl_2]^+[SbF_6]^-$ and its neutral counterpart $[AlCl_3]$, in the reaction and subsequently demonstrated the catalytic role of the intermolecular EF. The intermolecular EFs showed unique catalytic activity by enhancing the conventional LA catalysis as well as stabilising some of the dormant ionic structures involved in a pseudo-pericyclic pathway.[2,30]

The LA catalysed RCCOM proceeds *via* two pathways under thermal conditions as shown in Scheme 1. The other most used LAs include $GaCl_3$,[31] $FeCl_3$,[32] tropylium cations,[33] Brønsted acids,[34] and various other organic reagents.[35] Scheme 1 shows a [2+2] cycloaddition reaction in the carbonyl–olefin metathesis with a competing carbonyl–ene reaction pathway. The carbonyl–ene reaction pathway proceeds through a six-membered cyclic transition state (**TS1-LA**) where the β-hydrogen shifts from an olefin to carbonyl oxygen to generate the intermediate **I1-LA**. Subsequently, a hydroalkoxylation step yields an oxetane (**I2-LA**) as shown in Scheme 1. Alternatively, the thermal [2+2] cycloaddition, through **TS2-LA**, can also lead to the formation of the oxetane (**I2-LA**). The retro [2+2] cycloaddition of the oxetane results in the formation of the carbonyl–olefin metathesis product (**PD**).[36] The present study is focused on the catalysis imparted by the intermolecular EFs on the thermal [2+2] cycloaddition and carbonyl–ene reaction.

2. Computational details

All calculations were performed with the Gaussian 16 suite program.[37] All geometries were optimized at the B97-D[38,39] density functional theory (DFT) with the Def2-SVP basis set (B1).[40,41] Geometries were optimized at the SMD implicit solvation model considering 1,2-dichloroethane as the solvent.[42] Frequency calculations were performed at the B1 level of theory where the transition states (**TS**s) were characterised by one imaginary frequency corresponding to the reaction coordinate, whereas the reactants (**RC**s) and intermediates (**I**s) were devoid of any imaginary frequency. The intrinsic reaction coordinate (IRC) calculations were used for further verification of the optimized **TS**s.[43–45] Energies were further refined at the B97-D/Def2-TZVP[40] level of theory (B2) in a similar solvation model as in B1 optimization. The EF calculations were performed by single point calculations on the B1 optimized geometries at the B2 level of theory, as well as on geometries optimized at the B2 level of theory in the presence of the EF. The intermolecular EFs were quantified using the TITAN code.[46] Implicit solvation models in the present study under higher EFs are aimed to mimic the intermolecular EF generated by the LAs. However, such solvation models lack solvent specific charge transfers under high EFs[15,18] which are more relevant in a real reaction in solvents in an external EF experimental setup.

3. Results and discussion

The introduction of an LA into the RCCOM reaction results in efficient catalysis under mild experimental conditions.[47] The ion-pair ($[AlCl_2]^+[SbF_6]^-$) LA is generated from the precursors $AgSbF_6$ and $AlCl_3$ as an active catalyst for the reaction. The *in situ* generated LA acts as a strong Lewis acidic superelectrophile to stimulate relatively unreactive **RC** in RCCOM reactions as in Scheme 1.[36]

3.1. Quantification of the intermolecular EF and catalysis

The proximity of the LA can impart an extreme (>0.01 a.u.[5]) EF on the reactants and the resultant mechanistic changes that lead to catalysis are of prime importance.[48] The quantification of intermolecular EF as a function of LA proximity and its catalytic activity is summarised in Fig. 1. The equilibrium distance, defined as '*d*', between an aluminium atom in the LA ($[AlCl_2]^+[SbF_6]^-$) and the **RC** carbonyl oxygen (O_d) is 1.79 Å in

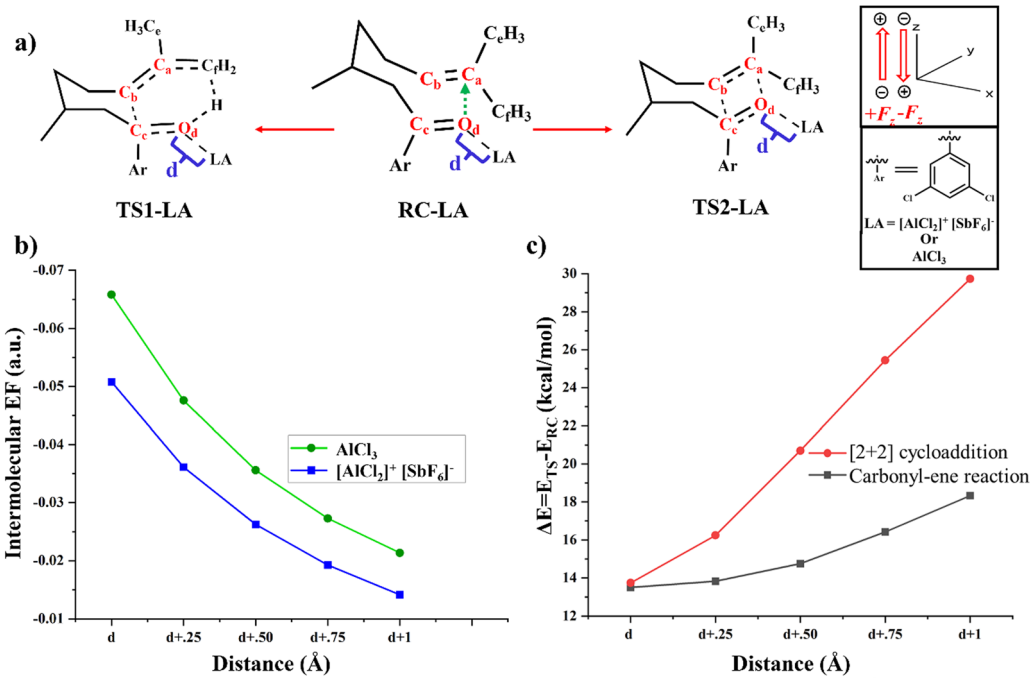

Fig. 1 Quantification of the intermolecular EFs and their catalytic activity. (a) Structural details of **RC-LA**, **TS1-LA** and **TS2-LA**. The green arrow denotes the reaction axis in **RC-LA**. (b) The intermolecular EFs (in a.u.) along the reaction axes as a function of LA proximity. The *x*-axis shows the LA distance from the **RC** (O_d–LA). The blue line shows intermolecular EFs for the $[AlCl_2]^+[SbF_6]^-$, and the green line shows intermolecular EFs for $AlCl_3$. (c) Energy barrier (ΔE) as a function of LA ($[AlCl_2]^+[SbF_6]^-$) distances. The black line shows ΔE for the carbonyl–ene reaction (ΔE = ($E_{\mathbf{TS1\text{-}LA}}$) − ($E_{\mathbf{RC\text{-}LA}}$)), and the red line represents ΔE for the [2+2] cycloaddition reaction (ΔE = ($E_{\mathbf{TS2\text{-}LA}}$) − ($E_{\mathbf{RC\text{-}LA}}$)). The '*d*' represents the equilibrium distances in Å (0.001 a.u. = 51.4 mV Å^{-1}).

both **RC-LA** and **TS1-LA**, while it is 1.74 Å in **TS2-LA**. In the case of LA ($AlCl_3$), the equilibrium distance '*d*' is found to be 1.82 Å in both **RC-LA** and **TS1-LA**, and 1.77 Å in **TS2-LA**. The proximity effect of the LA to the reactant was analysed by imposing manual displacement to the equilibrium distance '*d*' along the O_d–LA direction. Fig. 1b shows the amount of intermolecular EF along the reaction axis as a function of the proximity of the LA to the reactant. The intermolecular electric field (EF) is computed using the TITAN code, as illustrated in Fig. S1 in the ESI.† The intermolecular EF due to the LA is mapped onto the axis that starts from oxygen (O_d) and passes through the carbon (C_a) atom as shown in Fig. 1a. In the optimized geometry of the LA ($[AlCl_2]^+[SbF_6]^-$)-coordinated **RC**, the intermolecular EF along the reaction axis is −0.0507 a.u. and for LA ($AlCl_3$), the value is −0.0658 a.u. As the distance increases to (d + 1) Å, the intermolecular EF value decreases to −0.0141 a.u. for LA($[AlCl_2]^+[SbF_6]^-$) and −0.0213 a.u. for LA($AlCl_3$), respectively. The results also underscore that the use of an ion-pair ($[AlCl_2]^+[SbF_6]^-$) may not always bring enhanced intermolecular EF components along the reaction axis. The net intermolecular EF component along the reaction axis, which is a vector, depends on the relative orientation of charges in space. The intermolecular EF displays non-homogeneity within a reaction, suggesting a complex spatial dispersion of electrostatic forces.[49,50] The intermolecular EF value approaches near zero at a longer distance of LA as shown in Fig. 1b and Table S1 (ESI†).

Both carbonyl–ene and [2+2] cycloaddition reactions are catalysed by $AlCl_3$ and the $[AlCl_2]^+[SbF_6]^-$ ion-pair. However, the ion pair catalysed reaction has a lower energy barrier than its neutral counterpart. The energy barriers for the carbonyl–ene and [2+2] cycloaddition reactions are 14.1 and 14.4 kcal mol^{-1} respectively with the ion-pair LA catalyst and the barriers are further increased to 15.9 and 17.1 kcal mol^{-1} respectively with the $AlCl_3$ catalyst as shown in Fig. 1c and Fig. S2 in the ESI.† The lower energy barriers for the ion-pair catalyst, irrespective of having a lower magnitude of intermolecular EF along the reaction axis, are due to the enhanced Lewis acidity which is successively discussed in the article after detailing the EF catalysis. Fig. 1c displays the energy barrier of the $[AlCl_2]^+[SbF_6]^-$ catalysed reaction as a function of LA proximity. LA-[$AlCl_3$] also showed similar trends between the energy barrier and LA proximity (Fig. S3 in the ESI†). The separation between the **RC** and the LA directly impacts the energy barrier as shown in Fig. 1c. As the distance extends from the equilibrium distance '*d*' to (d + 1) Å, the ΔE increases from 13.27 kcal mol^{-1} to 18.02 kcal mol^{-1} for the carbonyl–ene reaction and from 13.73 kcal mol^{-1} to 29.61 kcal mol^{-1} for the [2+2] cycloaddition reaction (Table S2 in the ESI†). It should be noted that the barrier of the reaction shows a continuous increase as a function of distance between the **RC** and LA and it does not show any sudden increase while detaching the Lewis coordination. All in all, the distance between the **RC** and LA affects the catalysis, apart from the conventional LA coordination, by imparting an intermolecular EF along the reaction axis. The so-generated intermolecular EF also enhances, complementarily, the conventional LA catalysis (*vide infra*).

3.2. Origin of catalysis along the reaction axis due to the intermolecular EF

In RCCOM, the innate covalent structure of **RC-LA** needs to be changed to a more ionic structure to facilitate the reaction. The covalent electronic structure along with its ionic resonance structure is shown in Scheme 2. Even though the ionic resonance structure is not normally attainable, a properly oriented component of an intermolecular EF or an oriented external EF analogue can stabilise such dormant polar configurations and mix them into the covalent structure. Enhanced stabilisation of the ionic structure brings catalysis in carbonyl–ene reactions and facilitates a pseudo-pericyclic pathway for the thermal [2+2] cycloaddition reaction as detailed in the following discussion.

The LA coordination stabilises the negatively charged oxygen in the carbonyl–ene reaction, which abstracts the β-hydrogen atom present in the olefin group. The feasibility of both reactions in Scheme 2 is attributed to the stabilisation of the negative charge present in the O_d atom and the positive charge in C_a. The carbonyl–ene reaction proceeds through a concerted six-membered **TS** as shown in Scheme 2.[51] The π-orbital of the alkene, C_a=C_b, overlaps with the π*-orbital of the carbonyl C_c=O_d to form the C_b–C_c bond as shown in Fig. 2b. The molecular orbitals (MO) from a minimalistic model between formaldehyde and isobutene are displayed in Fig. 2b–d as the MOs of the LA coordinated RCCOM reaction are cumbersome. The presence of intermolecular EFs stabilises ionic structures and consequently changes C_a to become more cationic and O_d more anionic. During C_b–C_c bond formation, the reactant also undergoes a geometrical change to smoothen the abstraction of the allylic proton by the anionic O_d. The π* orbital of the carbonyl group (C_c=O_d) aligns with the σ* orbital of the C_f–H bond for a better overlap during the O_d–H bond formation in the concerted carbonyl–ene reaction. Orbital interactions in the carbonyl–ene reaction are shown in Fig. 2b. The geometrical changes are depicted in Fig. 2 where the dihedral angle, ω_1, undergoes a significant transition from 67.24° in **RC-LA** to 55.57° in **TS1-LA**, to form the C_b–C_c bond. Similarly, the changes in dihedral angles ω_2 and ω_3 by 7.93° and 3.14°, respectively, facilitate the overlap between the donor π*-orbital at the C_c–O_d and the acceptor C_f–H σ* orbital.

A pericyclic pathway for the concerted [2+2] cycloaddition is thermally forbidden.[52] Instead, the reaction proceeds *via* an ionic pseudo-pericyclic pathway as given in Scheme 2. The [2+2] cycloaddition proceeds with the formation of two new bonds between C_b and C_c and between C_a and O_d as shown in Fig. 2c and d. Along with the C_b–C_c bond formation, the nonbonding orbitals at the O_d atom, which is perpendicular to the C_c=O_d π-orbital, rotate and form a bond with the cationic C_a. The overlap of the nonbonding orbital at the O_d and the vacant p-orbital at the C_a atom leads to the bond formation and it does not require either C_a=C_b or C_c=O_d bonds to rotate 180°. The partial rotation of the nonbonding orbital at the O_d atom and the vacant p-orbital at the C_a atom plays a crucial role in facilitating the C_a–O_d bond formation and the corresponding transition state (**TS2-LA**) is depicted in Fig. 2d. The angle ω_1 undergoes a significant transition from 67.24° in the initial **RC-LA** to 36.59° in the subsequent **TS2-LA** indicating the rotation of the nonbonding orbital towards the vacant p-orbitals at the C_a atom. Similarly, angles ω_2 and ω_3 experience shifts of 29.30° and 19.65°, respectively, where the rotations facilitate overlap of the donor nonbonding orbital at the O_d and the acceptor vacant p-orbital at the C_a atom.

3.2.1. Results with an oriented external EF. To ascertain the sole role of EF in the reaction, we considered the pristine reaction without the coordinated LA. The oriented external EF is applied along the reaction axis in **RC** and **TS**s akin to the intermolecular EF's magnitude and directions. As depicted in Fig. 3, the energy barrier decreases while the oriented external EF intensity increases along the axis that starts from oxygen (O_d) and passes through the carbon (C_a) atom. The barriers for

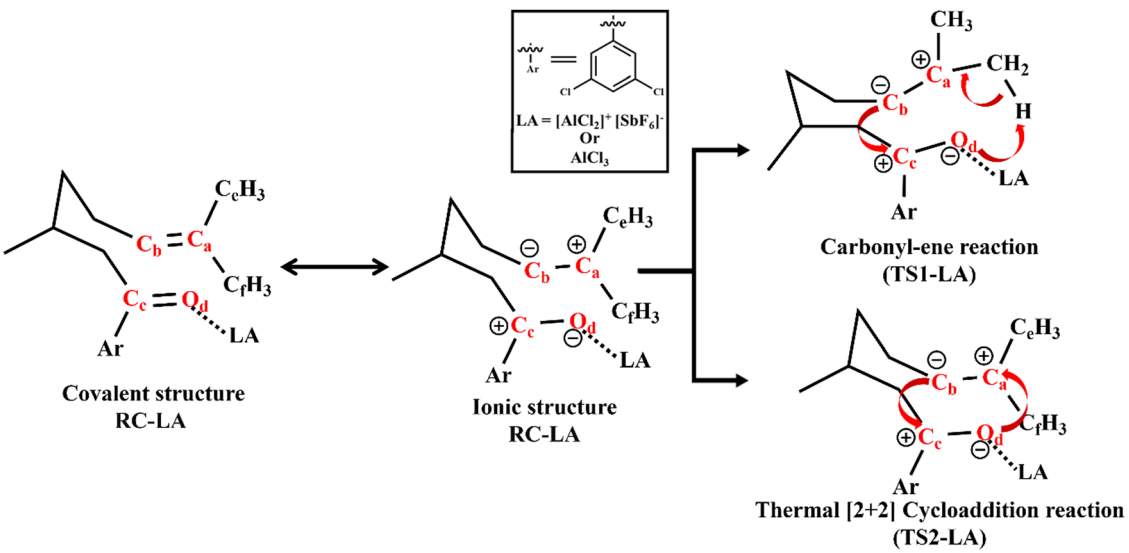

Scheme 2 Thermal [2+2] cycloaddition and carbonyl–ene reaction that proceeds through a dormant ionic structure.

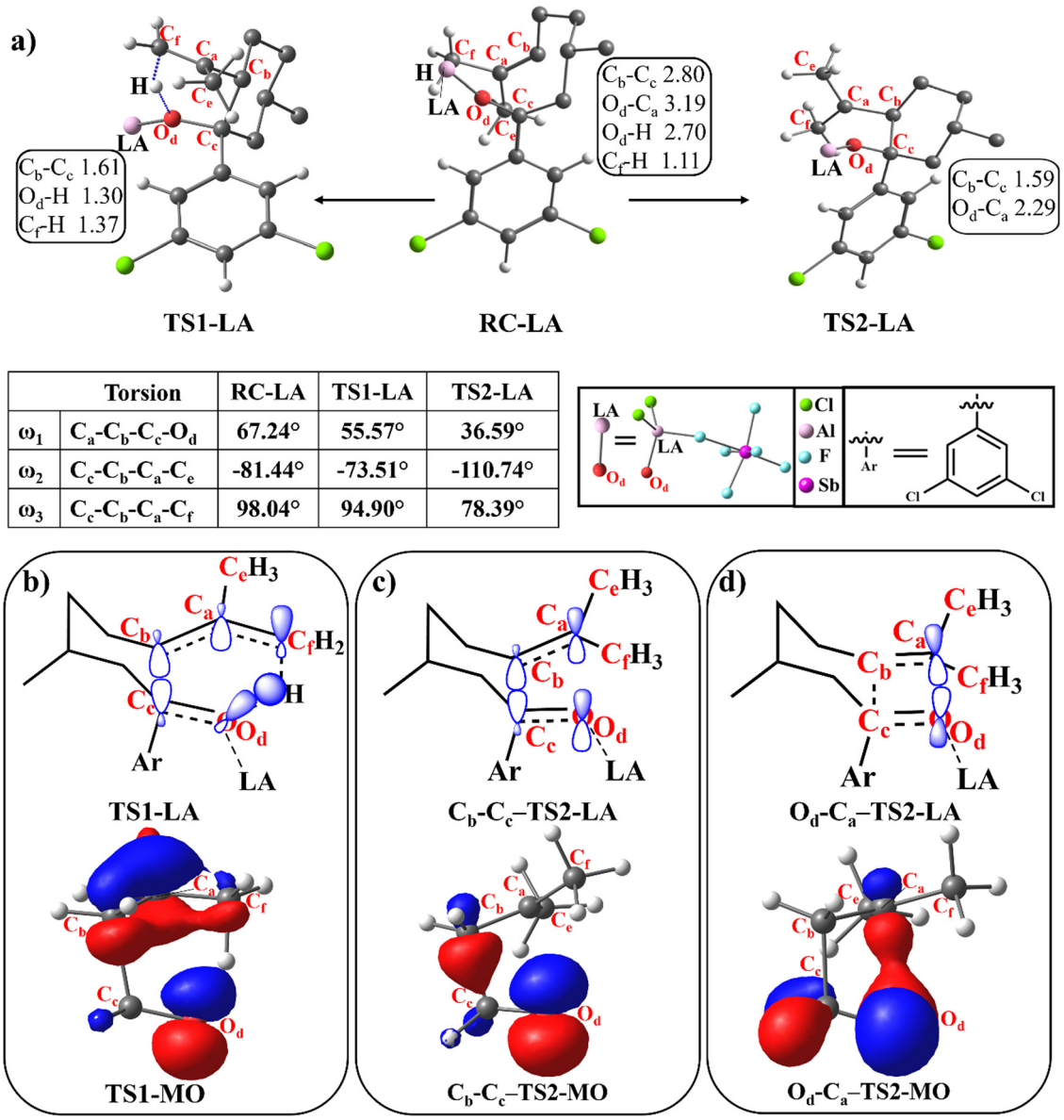

	Torsion	RC-LA	TS1-LA	TS2-LA
ω_1	C_a-C_b-C_c-O_d	67.24°	55.57°	36.59°
ω_2	C_c-C_b-C_a-C_e	-81.44°	-73.51°	-110.74°
ω_3	C_c-C_b-C_a-C_f	98.04°	94.90°	78.39°

Fig. 2 Geometrical and electronic structural details of the carbonyl–ene and [2+2] cycloaddition pathways. (a) The structural changes of **TS1-LA** and **TS2-LA** from the **RC-LA**. (b) The MO interaction at the **TS1-LA** for C_b–C_c and O_d–H bond formation along with the model system. (c) The MO interaction at the **TS2-LA** for the C_b–C_c bond formation. (d) The MO interaction at the **TS2-LA** for the O_d–C_a bond formation. Distances are given in Å and the torsional changes are given in degrees. Nonsignificant H-atoms are removed for clarity. All iso values are maintained at 0.06.

the pristine carbonyl–ene and [2+2] cycloaddition reaction in the absence of LA were found to be prohibitively high at 30.0 kcal mol^{-1} and 48.9 kcal mol^{-1} respectively as shown in Fig. 3b. As seen from the relative energy values in Fig. 3c, the **RC** is stabilised under both $+F_z$ and $-F_z$ as compared to the zero-field. Relative energies of the **TS**s also decreased along the $-F_z$ direction. However, both **TS1** and **TS2** destabilised along the $+F_z$ direction up to 0.004 a.u. and 0.009 a.u. respectively before the resurgence of stabilisation as shown in Fig. 3c and Table S3 in the ESI.† The existence of the highest destabilisation point for the **TS** is due to the two-way electron transfer mechanism as shown in Scheme 2 which is similar to the earlier reports on electrostatic resistance point (ERP).[17,53] The ERP is characterised by the zero-dipole moment component along the *z*-axis (μ_z) of the **TS**s and **RC** as shown in Fig. 3d and Table S4 in the ESI.†

A comparison of the changes in relative energies of **RC** and **TS**s explains the observed catalysis along the $-F_z$ direction and inhibition along the $+F_z$ direction. (Fig. 3b and c) Under −0.02 a.u. oriented external EF, ΔE decreases to 20.3 kcal mol^{-1} for the carbonyl–ene reaction and up to 17.7 kcal mol^{-1} for the [2+2] cycloaddition reactions. Conversely, with a +0.02 a.u. oriented external EF along the reaction axis, ΔE increases to 35.4 kcal mol^{-1} for the carbonyl–ene reaction and up to 72.1 kcal mol^{-1} for the [2+2] cycloaddition reaction (Table S5 in the ESI†). The relative stabilisation of **TS**s along $-F_z$ is higher as

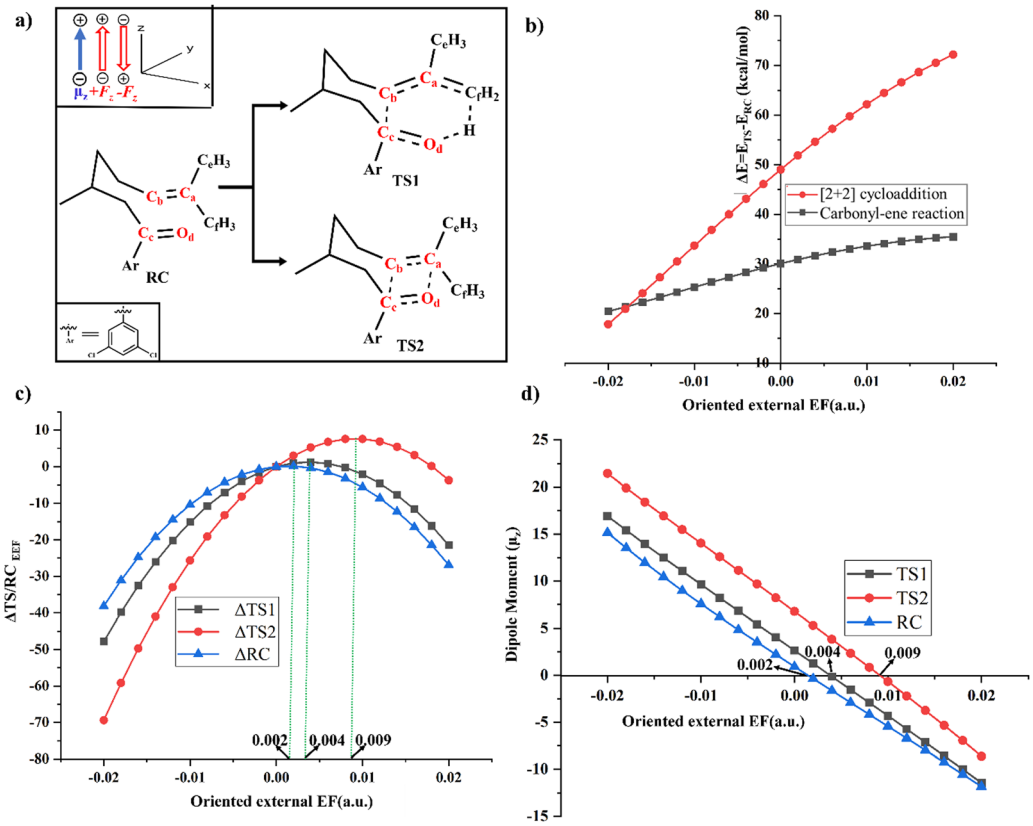

Fig. 3 The effect of an oriented external EF on catalysis for the RCCOM reaction. (a) Schematic representation for application of the oriented external EF in the RCCOM reaction. (b) Plot between the reaction barrier energy and oriented external EF. The black line represents the barrier energy ($\Delta E = E_{\mathbf{TS1}} - E_{\mathbf{RC}}$) for the carbonyl–ene reaction, while the red line depicts the barrier energy ($\Delta E = E_{\mathbf{TS2}} - E_{\mathbf{RC}}$) for the [2+2] cycloaddition as a function of the oriented external EFs. (c) Plot between the relative energy changes of **TS1** (black), **TS2** (red), and **RC** (blue) to the applied oriented external EF. $\Delta\mathbf{TS/RC}_{\mathrm{EEF}} = E(\mathbf{TS/RC}_{\mathrm{applied\,EEF}}) - E(\mathbf{TS/RC}_{\mathrm{zero\,EEF}})$. (d) The dipole moment component along the reaction axis (μ_z) is plotted against the oriented external EF values (0.001 a.u. = 51.4 mV Å^{-1}).

compared to the **RC** and *vice versa* along the $+F_z$ direction effectively resulting in catalysis along the $-F_z$ direction and inhibition along the $+F_z$ direction.

3.2.2. How do oriented EFs modulate molecular orbitals for carbonyl–ene and [2+2] cycloaddition reactions under thermal conditions? The oriented external EF also facilitates the ionic pathways in both carbonyl–ene and [2+2] cycloaddition reactions as shown in Fig. 3 which is similar to the LA catalysed mechanism as detailed in Fig. 2. The extent of asynchronicity in the [2+2] cycloaddition and carbonyl–ene reaction depends on the direction and amount of oriented external EF. The anionic character of the carbonyl oxygen (O_d) atom is enhanced when exposed to oriented external EFs in the $-F_z$ direction. At the same time, it diminishes when the EF is applied in the $+F_z$ direction. This variation is reflected in the NBO charges at the O_d atom, which shift from −0.78 to −0.57 in transition state **TS1** and from −0.89 to −0.61 in **TS2** under external EFs of −0.02 a.u. and +0.02 a.u., respectively, as illustrated in Fig. S4 and Table S6 in the ESI.† Moreover, the oriented external EF influences the concerned reaction coordinates as evidenced by the bond distances at the **TS**s. For example, in **TS1**, the application of a $-F_z$ field decreases the distance between the C_b and C_c atoms while increasing the O_d–H bond distance and *vice versa* occurs under the $+F_z$ field. Within a range of oriented external EF from +0.01 a.u. to −0.01 a.u., the C_b–C_c bond distance contracts from 2.47 Å to 1.71 Å, while the O_d–H bond distance expands from 1.12 Å to 1.45 Å as displayed in Fig. S5 in the ESI.†

Oriented external EF, analogous to LA, possesses the capability to bring asynchronous **TS**s and partially rotate the orbitals to proceed with reactions more effectively as shown in Fig. 4. In **TS1**, the angular displacement of ω_4 experiences a notable variation from 57.90° to 57.44° in response to changes in oriented external EF strength, ranging from 0.01 ($+F_z$) to −0.01 ($-F_z$). Additionally, angles ω_5 and ω_6 undergo shifts of −4.71° and 0.69°, respectively. The changes in ω_5 facilitate the rotation of the C_fH_3 group that enables the interaction between the π*-orbital of the C_c–O_d atom and the σ* orbital of C_f–H and reduces the energy barrier for **TS1**.

The angle ω_4 as defined in Fig. 4 undergoes a significant transition from 21.35° to 39.93° in **TS2** as the amount of oriented external EF varies from 0.01($+F_z$) to −0.01($-F_z$) for the [2+2] cycloaddition reaction. Additionally, the angles ω_5 and ω_6 in **TS2** also change by 12.18° and −8.08° respectively. The changes in ω_6, an improper dihedral angle, indicate that the $-F_z$ tends to promote a more planar cationic structure for

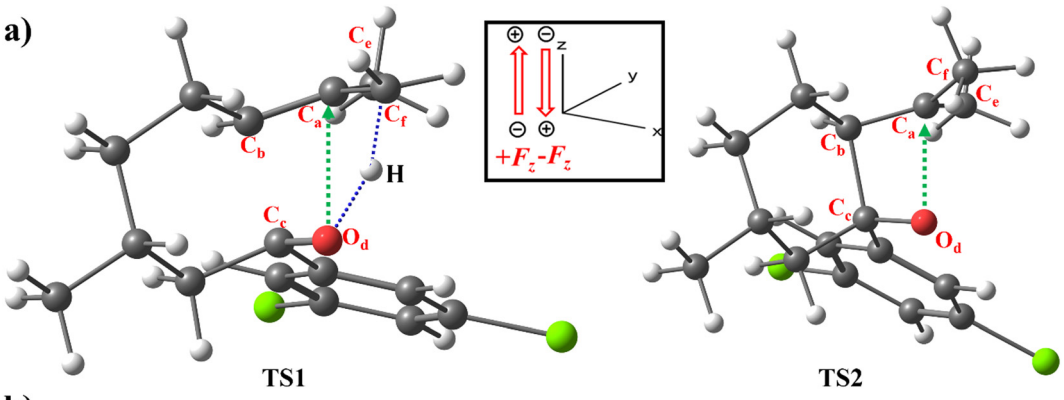

b)

Torsion		TS1			TS2		
		0.01a.u.	-0.01a.u.	Difference	0.01a.u.	-0.01a.u.	Difference
ω_4	C_a-C_b-C_c-O_d	57.90°	57.44°	0.46°	21.35°	39.93°	-18.58°
ω_5	C_c-C_b-C_a-C_f	-71.23°	-66.52°	-4.71°	97.02°	84.84°	12.18°
ω_6	C_a-C_e-C_b-C_f	-6.27°	-6.96°	0.69°	-15.59°	-7.51°	-8.08°

Fig. 4 The effect of oriented external EF in the carbonyl–ene and [2+2] cycloaddition reactions. (a) The optimized geometries of **TS1** and **TS2** at the B1 level of theory under zero field. (b) The torsional angle changes for the carbonyl–ene (**TS1**) and [2+2] cycloaddition (**TS2**) reactions under an oriented external EF (0.001 a.u. = 51.4 mV Å^{-1}).

the C_a atom. As in Fig. 2 the changes due to the $-F_z$ EF in ω_4 and ω_5 facilitate a better overlap of the O_d nonbonding orbital to the vacant p-orbital at the C_a. As such, the EF along $-F_z$ sets the foundation for a better rotation of the donor O_d nonbonding orbital and the acceptor vacant p-orbital, leading to the O_d–C_a bond formation and effectively bringing down the barrier in **TS2**. Geometric comparison between **TS1** and **TS2** shows that **TS1** requires less substantial structural changes and directly correlates with its lower energy. Thus, in the progression of the reaction, the change in the dihedral angle plays a pivotal role in facilitating molecular transformations. It orchestrates the rotation of both the nonbonding donor orbital and the vacant acceptor p-orbital for a smooth pseudo-pericyclic pathway.

An oriented external EF applied along the reaction axis has a direct impact on the energy difference between the lowest unoccupied molecular orbital ($LUMO_{(C=O)}$) and the highest occupied molecular orbital ($HOMO_{(C=C)}$).[54] The $HOMO_{(C=C)}$ overlaps with the $LUMO_{(C=O)}$ during the C_b–C_c bond formation. To detail the orbital energy changes, the **RC** was divided into two segments: the ene part and the carbonyl part. To preserve valency, hydrogen atoms were added to both the carbonyl and ene groups as given in Fig. 5a. The impact

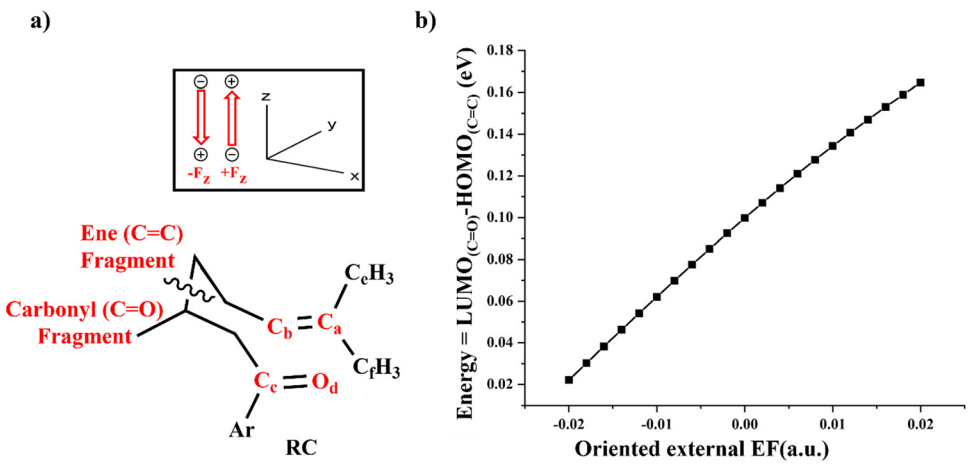

Fig. 5 The $LUMO_{(C=O)}$–$HOMO_{(C=C)}$ energy gap as a function of the oriented external EF. (a) The fragmentation scheme into carbonyl and ene units. (b) The change in the LUMO–HOMO energy gap with the oriented external EF. The *x*-axis denotes the oriented external EF (a.u.) and the *y*-axis represents the $LUMO_{(C=O)}$–$HOMO_{(C=C)}$ energy of **RC** (0.001 a.u. = 51.4 mV Å^{-1}).

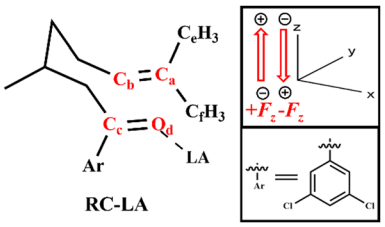

LA	$AlCl_3$	$[AlCl_2]^+[SbF_6]^-$
ΔE (carbonyl-ene reaction)	**15.9**	**14.1**
ΔE ([2+2]cycloaddition)	**17.1**	**14.4**
Intermolecular EF	**-0.065**	**-0.050**
Energy ($LUMO_{(LA)}$-$HOMO_{(LA)}$)	**0.217**	**0.081**

Fig. 6 A comparison between two LAs, $AlCl_3$ and $[AlCl_2]^+[SbF_6]^-$, showcasing their energy barriers in kcal mol^{-1} ($\Delta E = E_{TS\text{-}LA} - E_{RC\text{-}LA}$), intermolecular EF in a.u., and the LUMO–HOMO energy gap in eV (0.001 a.u. = 51.4 mV Å^{-1}).

of an oriented external EF on the MOs of carbonyl and ene groups was measured by considering one group at a time and keeping similar relative orientation of external EF to that in Fig. 5. The ene group is replaced with a dummy atom (see Fig. S6 in the ESI†) to study the EF's effect on the MOs of the carbonyl group and *vice versa* for the ene group.[55] EF analysis between the ene and carbonyl fragments showed that application of external EF along the $+F_z$ direction increased the LUMO–HOMO energy gap, whereas applying it along the $-F_z$ direction decreased the energy gap as visible in Fig. 5b and Table S7 in the ESI.†

3.3. How does the catalytic component of intermolecular EF add to Lewis acidity?

A comparative analysis of the LAs, $AlCl_3$ and $[AlCl_2]^+[SbF_6]^-$, revealed that $[AlCl_2]^+[SbF_6]^-$ consistently shows a lower ΔE value in both carbonyl–ene and [2+2] cycloaddition reactions, as depicted in Fig. 6. Surprisingly, the component of intermolecular EF along the axis that connects O_d to C_a is higher for $AlCl_3$ (−0.06 a.u.) than that for $[AlCl_2]^+[SbF_6]^-$ (−0.05 a.u.). This result underscores that merely creating ionic fragments may not lead to enhanced EF catalysis, as the strength of intermolecular EF components along a specific bond or reaction axis depends not only on the magnitude of the charges but also on the relative orientations of the charged groups. Comparison of the LUMO–HOMO energy gaps of the LAs revealed a notable distinction between $AlCl_3$ and $[AlCl_2]^+[SbF_6]^-$ where the former has a higher 0.217 eV energy gap against 0.081 eV of the latter. The LUMO–HOMO energy gap is an indicator of Lewis acidity, suggesting that a lower value, as seen in ion pairs, represents a more acidic nature than $AlCl_3$.[56,57] The reduced intermolecular EF catalysis along the reaction axis is compensated by the enhanced Lewis acid catalysis.

A complete picture of the catalytic cycle and the effect of the oriented external EF on the reaction is shown in Fig. 7. The oriented external EF is applied along the reaction axis, parallel to the electron flow in the reaction mechanism. The oriented

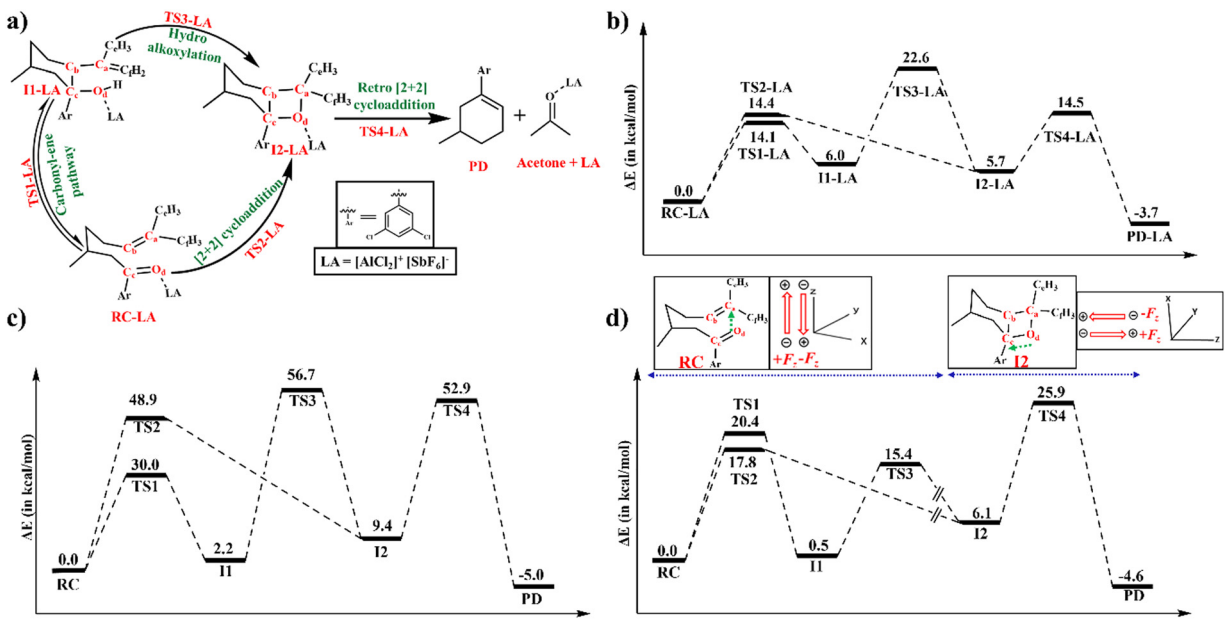

Fig. 7 The catalytic contribution of the oriented external EF in the RCCOM reaction. (a) The catalytic cycle of the RCCOM reaction. (b) Energy profile of the ion-pair catalysed RCCOM reaction. (c) Energy profile of the pristine RCCOM reaction. (d) Energy profile of the pristine RCCOM reaction in the presence of an oriented external EF of $F_z = -0.02$ a.u. The energy values in kcal mol^{-1} are provided at the B2 level of theories. The direction of the z-axis is redefined from **I2** onwards as given in the figure inset (0.001 a.u. = 51.4 mV Å^{-1}).

external EF is applied along O_d to C_a in **TS1**, **TS2**, and **TS3**, whereas in **TS4**, the direction of F_z is changed from O_d to C_c to make it parallel to the reaction axis of the retro [2+2] cycloaddition step. Fig. 7a illustrates all the individual steps in the catalytic cycle while Fig. 7b represents the corresponding potential energy profile. The preferred pathway in Fig. 7b, where the ion pair is coordinated to **RC**, proceeds through **TS2-LA**, **I2-LA**, and **TS4-LA** to the metathesis product. Due to the lower barrier of the carbonyl–ene pathway (**TS1-LA**), **I1-LA** remains in equilibrium with **RC-LA**. However, the following hydroalkoxylation step towards **I2-LA** is not operative due to the higher barrier. Fig. 7c and Table S8 in the ESI† depict the energy profile of the pristine reaction without any oriented external EF or LA where barriers are found to be prohibitively high. The profile in Fig. 7d is recreated by aligning an oriented external EF along the reaction axis at each individual step to mimic the intermolecular EF component along the reaction axes. Applying an oriented external EF along the reaction axis, specifically along the O_d–C_a direction, catalyses the carbonyl–ene reaction, hydroalkoxylation, and [2+2] cycloaddition. Similarly, in the retro [2+2] cycloaddition reaction, where the electron flow is along the O_d–C_c direction, the reaction is catalysed by an oriented external EF aligned in that direction. The component of intermolecular EF along the O_d–C_c bond in **I2** is found to be −0.08 a.u. As such, the application of an EF along the reaction axis profoundly influences the catalytic efficiency in the carbonyl–ene reaction, hydroalkoxylation, [2+2] cycloaddition, and retro [2+2] cycloaddition. It also conveys that the intermolecular EF component along the reaction axis, which originates from the LAs, has a unique catalytic effect.

The intermolecular EF generated at the reaction site is nonuniform and its effect and magnitude diminish significantly for groups and atoms located farther from the LA catalyst. In contrast, the externally applied EF is uniform which exerts the same magnitude of influence on all groups and atoms along its applied direction. Due to this difference between uniform external and nonuniform intermolecular EFs, a lower magnitude of external EF is enough to reproduce similar catalytic characteristics by an intermolecular EF. For example, an external EF of 0.022 a.u. is enough to lower the pristine reaction barrier to match that of the LA-catalysed [2+2] cycloaddition reaction where the latter has an intermolecular EF of 0.050 a.u. All in all, along with the conventional LA catalysis characterised by the LUMO–HOMO energies, the intermolecular EF originating from LAs has a distinct and unique contribution towards gross catalysis.

4. Conclusion

Exploring the thermal [2+2] cycloaddition and carbonyl–ene reactions in a ring-closing carbonyl–olefin metathesis (RCCOM) sheds light on the pivotal roles of intermolecular EFs in catalysis. The specific orientations of coordinated LAs with reactants lead to the generation of specifically oriented intermolecular EF components along the reaction axis. Intermolecular EF components along the reaction axis, which is parallel to the electron flow in each reaction step, are found to catalyse the reaction with a unique mechanism. The preferred pathway for the reaction is a [2+2] cycloaddition followed by a retro [2+2] cycloaddition step. A carbonyl–ene reaction step is also operative which makes the starting reactant form an equilibrium with the following intermediate. In the thermal [2+2] cycloaddition, the intermolecular EF promotes the charge transfer from the alkene (C═C π-orbital) donor to the carbonyl (C═O π*-orbital) acceptor to enhance the C–C bond formation. Stabilisation of the resultant charge transferred ionic intermediates further enhances the subsequent C–O bond formation *via* a partial rotation of nonbonding electrons on oxygen which is necessary to circumvent the thermal forbiddances of [2+2] cycloaddition.

The carbonyl–ene reaction also follows the initial step of C–C bond formation as in [2+2] cycloaddition and accumulates anionic charge on the carbonyl oxygen. Subsequent O_d–H bond formation proceeds *via* electron transfer to the σ* orbital of the C_f–H bond. The mechanistic importance of intermolecular EF is delineated by modelling reactions under similarly oriented external EFs. Quantification of the intermolecular EF along the reaction axis has revealed that, contrary to common assumption, the neutral LA($[AlCl_3]$) imparts a higher intermolecular EF than its ion pair ($[AlCl_2]^+[SbF_6]^-$) counterpart. The findings exemplify that judicious utilisation of intermolecular EFs can effectively maximize catalytic benefits and a catalytic mechanism is incomplete without delineating the role of intermolecular EFs.

Conflicts of interest

The authors declare no conflicts.

Acknowledgements

RR acknowledges the Science and Engineering Research Board (SERB), India, for the grant SRG/2021/000439. LS and KG acknowledge teaching assistantships from NITR.

References

1 S. Shaik, D. Mandal and R. Ramanan, *Nat. Chem.*, 2016, **8**, 1091–1098, DOI: **10.1038/nchem.2651**.
2 S. Shaik, R. Ramanan, D. Danovich and D. Mandal, *Chem. Soc. Rev.*, 2018, **47**(14), 5125–5145, DOI: **10.1039/c8cs00354h**.
3 S. Ciampi, N. Darwish, H. M. Aitken, I. Diez-Perez and M. L. Coote, *Chem. Soc. Rev.*, 2018, **47**, 5146–5164, DOI: **10.1039/C8CS00352A**.
4 A. C. Aragonès, N. L. Haworth, N. Darwish, S. Ciampi, N. J. Bloomfield, G. G. Wallace, I. Diez-Perez and M. L. Coote, *Nature*, 2016, **531**(7592), 88–91, DOI: **10.1038/nature16989**.
5 S. D. Fried, S. Bagchi and S. G. Boxer, *Science*, 2014, **346**(6216), 1510–1514, DOI: **10.1126/science.1259802**.

6 A. Warshel, *Acc. Chem. Res.*, 1981, **14**(9), 284–290, DOI: 10.1021/ar00069a004.
7 R. Meir, H. Chen, W. Lai and S. Shaik, *ChemPhysChem*, 2010, **11**(1), 301–310, DOI: 10.1002/cphc.200900848.
8 Z. Wang, D. Danovich, R. Ramanan and S. Shaik, *J. Am. Chem. Soc.*, 2018, **140**(41), 13350, DOI: 10.1021/jacs.8b08233.
9 H. Hirao, H. Chen, M. A. Carvajal, Y. Wang and S. Shaik, *J. Am. Chem. Soc.*, 2008, **130**, 3319–3327, DOI: 10.1021/ja070903t.
10 R. Ramanan, D. Danovich, D. Mandal and S. Shaik, *J. Am. Chem. Soc.*, 2018, **140**, 4354–4362, DOI: 10.1021/jacs.8b00192.
11 G. Cassone, F. Pietrucci, F. Saija, F. Guyot and A. M. Saitta, *Chem. Sci.*, 2017, **8**, 2329–2336.
12 A. Yosipof, H. Basch and S. Hoz, *J. Phys. Chem. A*, 2013, **117**, 5023–5027, DOI: 10.1021/jp402758u.
13 T. Stuyver, D. Danovich, F. De Proft and S. Shaik, *J. Am. Chem. Soc.*, 2019, **141**(24), 9719–9730, DOI: 10.1021/jacs.9b04982.
14 V. Conti Nibali, S. Maiti, F. Saija, M. Heyden and G. Cassone, *J. Chem. Phys.*, 2023, **158**, 184501.
15 S. Pullanchery, S. Kulik, T. Schönfeldová, C. K. Egan, G. Cassone, A. Hassanali and S. Roke, *Nat. Commun.*, 2024, **15**, 5951.
16 K. Gopakumar, V. Samantaray, M. K. Prusty, L. Swain and R. Ramanan, *Chem. Commun.*, 2023, **2**, 13054–13057, DOI: 10.1039/D3CC04283A.
17 G. Cassone, A. Sofia, G. Rinaldi and J. Sponer, *J. Phys. Chem. C*, 2019, **123**, 9202–9208.
18 G. Cassone and F. Martelli, *Nat. Commun.*, 2024, **15**, 1856.
19 H. Hao, I. Leven and T. Head-Gordon, *Nat. Commun.*, 2022, **13**, 280, DOI: 10.1038/s41467-021-27941-x.
20 C. Zhu, L. N. Pham, X. Yuan, H. Ouyang, M. L. Coote and X. Zhang, *J. Am. Chem. Soc.*, 2023, **145**(39), 21207–21212, DOI: 10.1021/jacs.3c08818.
21 P. Basuri, L. E. Gonzalez, N. M. Morato, T. Pradeep and R. G. Cooks, *Chem. Sci.*, 2020, **11**, 12686–12694, DOI: 10.1039/D0SC02467H.
22 E. Gnanamani, X. Yan and R. N. Zare, *Angew. Chem., Int. Ed.*, 2020, **59**, 3069–3072, DOI: 10.1002/anie.201913069.
23 Z. P. Rao, Y. G. Fang, Y. S. Pan, W. C. Yu, B. L. Chen, J. S. Francisco, C. Q. Zhu and C. H. Chu, *J. Am. Chem. Soc.*, 2023, **145**(45), 24717–24723, DOI: 10.1021/jacs.3c08101.
24 X. Song, C. Basheer and R. N. Zare, *J. Am. Chem. Soc.*, 2023, **145**(50), 27198–27204, DOI: 10.1021/jacs.3c08643.
25 G. Cassone, *J. Phys. Chem. Lett.*, 2020, **11**, 8983–8988.
26 D. Zhang, X. Yuan, C. Gong and X. Zhang, *J. Am. Chem. Soc.*, 2022, **144**(35), 16184–16190, DOI: 10.1021/jacs.2c07385.
27 K. Gong, A. Nandy, Z. Song, Q.-S. Li, A. Hassanali, G. Cassone, S. Banerjee and J. Xie, *J. Am. Chem. Soc.*, 2024, **146**(46), 31585–31596.
28 I. K. Mati and S. L. Cockroft, *Chem. Soc. Rev.*, 2010, **39**(11), 4195–4205, DOI: 10.1039/B822665M.
29 T. Stuyver, R. Ramanan, D. Mallick and S. Shaik, *Angew. Chem., Int. Ed.*, 2020, **59**(20), 7915, DOI: 10.1002/anie.201916592.
30 H. Schmalzried and S. Smolin, *Ber. Bunsen-Ges. Phys. Chem.*, 1998, **102**, 1740–1746, DOI: 10.1002/bbpc.19981021203.
31 H. Albright, H. L. Vonesh, M. R. Becker, B. W. Alexander, J. R. Ludwig, R. A. Wiscons and C. S. Schindler, *Org. Lett.*, 2018, **20**, 4954–4958, DOI: 10.1021/acs.orglett.8b02086.
32 J. R. Ludwig, S. Phan, C. C. McAtee, P. M. Zimmerman, J. J. Devery and C. S. Schindler, *J. Am. Chem. Soc.*, 2017, **139**, 10832–10842, DOI: 10.1021/jacs.7b05641.
33 U. P. N. Tran, G. Oss, D. P. Pace, J. Ho and T. V. Nguyen, *Chem. Sci.*, 2018, **9**, 5145, DOI: 10.1039/C8SC00907D.
34 T. Malakar and P. M. Zimmerman, *J. Org. Chem.*, 2021, **86**(3), 3008–3016, DOI: 10.1021/acs.joc.0c03021.
35 L. Ravindar, R. Lekkala, K. P. Rakesh, A. M. Asiri, H. M. Marwani and H.-L. Qin, *Org. Chem. Front.*, 2018, **5**, 1381–1391, DOI: 10.1039/C7QO01037K.
36 A. J. Davis, R. B. Watson, D. J. Nasrallah, J. L. Gomez-Lopez and C. S. Schindler, *Nat. Catal.*, 2020, **3**, 787–796, DOI: 10.1038/s41929-020-00499-5.
37 M. J. Frisch, G. W. Trucks, H. B. Schlegel, G. E. Scuseria, M. A. Robb, J. R. Cheeseman, G. Scalmani, V. Barone, B. Mennucci and G. A. Petersson, *Gaussian16, Revision A.03*, Gaussian Inc, Wallingford CT, 2016[See ESI† for full reference].
38 S. Grimme, *J. Comput. Chem.*, 2006, **27**, 1787–1799, DOI: 10.1002/jcc.20495.
39 S. Grimme, *J. Chem. Phys.*, 2006, **124**, 034108, DOI: 10.1063/1.2148954.
40 F. Weigend and R. Ahlrichs, *Phys. Chem. Chem. Phys.*, 2005, **7**, 3297, DOI: 10.1039/b508541a.
41 A. Schäfer, H. Horn and R. Ahlrichs, *J. Chem. Phys.*, 1992, **97**, 2571, DOI: 10.1063/1.463096.
42 A. V. Marenich, C. J. Cramer and D. G. Truhlar, *J. Phys. Chem. B*, 2009, **113**, 6378–6396, DOI: 10.1021/jp810292n.
43 K. Fukui, *Acc. Chem. Res.*, 1981, **14**, 363–368, DOI: 10.1021/ar00072a001.
44 C. Gonzalez and H. B. Schlegel, *J. Chem. Phys.*, 1989, **90**, 2154–2161, DOI: 10.1063/1.456010.
45 C. Gonzalez and H. B. Schlegel, *J. Phys. Chem.*, 1990, **94**, 5523–5527, DOI: 10.1021/j100377a021.
46 T. Stuyver, J. Huang, D. Mallick, D. Danovich and S. Shaik, *J. Comput. Chem.*, 2020, **41**(1), 74–82, DOI: 10.1002/jcc.26072.
47 H. Albright, A. J. Davis, J. L. Gomez-Lopez, H. L. Vonesh, P. K. Quach, T. H. Lambert and C. S. Schindler, *Chem. Rev.*, 2021, **121**, 9359–9406, DOI: 10.1021/acs.chemrev.0c01096.
48 J. L. Alvarez-Hernandez, X. Zhang, K. Cui, A. P. Deziel, S. Hammes-Schiffer, N. Hazari, N. Piekut and M. Zhong, *Chem. Sci.*, 2024, **15**(18), 6800–6815, DOI: 10.1039/D3SC06177A.
49 T. A. Rokob, I. Bakó, A. Stirling, A. Hamza and I. Pápai, *J. Am. Chem. Soc.*, 2013, **135**, 4425–4437, DOI: 10.1021/ja312387q.
50 S. Grimme, H. Kruse, L. Goerigk and G. Erker, *Angew. Chem., Int. Ed.*, 2010, **49**, 1402–1405, DOI: 10.1002/anie.200905484.
51 H. A. Rodríguez, D. A. Cruz, J. I. Padrón and I. Fernández, *J. Org. Chem.*, 2023, **88**, 11102–11110, DOI: 10.1021/acs.joc.3c01059.

52 R. Hoffmann and R. B. Woodward, *Acc. Chem. Res.*, 1968, **1**, 17–22, DOI: **10.1021/ar50001a003**.
53 K. Gopakumar, S. Shaik and R. Ramanan, *Angew. Chem., Int. Ed.*, 2023, **135**, e202307579, DOI: **10.1002/ange.202307579**.
54 S. Shaik, D. Danovich, J. Joy, Z. Wang and T. Stuyver, *J. Am. Chem. Soc.*, 2020, **142**(29), 12551–12562, DOI: **10.1021/jacs.0c05128**.
55 R. J. Burns, I. K. Mati, K. B. Muchowska, C. Adam and S. L. Cockroft, *Angew. Chem., Int. Ed.*, 2020, **59**(38), 16717–16724, DOI: **10.1002/anie.202006943**.
56 R. G. Parr and R. G. Pearson, *J. Am. Chem. Soc.*, 1983, **105**(26), 7512–7516, DOI: **10.1021/ja00364a005**.
57 W. B. J. C. R. Jensen, *Chem. Rev.*, 1978, **78**(1), 1–22, DOI: **10.1021/cr60311a002**.